Journal Name

ARTICLE

Spectroscopic Raman characterization of rutherfordine: a combined DFT and experimental study†

Received 00th January 20xx,
Accepted 00th January 20xx

DOI: 10.1039/x0xx00000x

www.rsc.org/

L. J. Bonales[a*], F. Colmenero[b], J. Cobos[a] and V. Timón[b]

A rutherfordine mineral was studied by means of Raman spectroscopy combined with first principle calculations based on density functional theory (DFT) method. A pseudopotential of uranium atom was generated and its performance was evaluated for a series of uranium-containing minerals. The structure of rutherfordine was determined for two symmetries (Pmmn and Imm2) and the resulting lattice parameters, bond lengths, bond angles, and X-Ray powder diffractogram were found in very good agreement with experimental values. The Raman spectrum was experimentally determined in the range 0-1700 cm^{-1} and calculated using density functional perturbation theory. The non-scaled theoretical wavenumbers also agree with the experimental values, therfore a detailed interpretation of the theoretical spectra allows us to assign the Raman bands found in the experimental spectrum.

1 Introduction

The performance of the final repository for spent nuclear fuel (SNF) as a deep geological repository requires the knowledge of the behavior of this waste after storage times of the order of some thousands of years.[1] It is widely accepted that after such long times the barriers that protect the waste will be breached and SNF will be in contact with water.[2] The matrix of the spent nuclear fuel composed by uranium dioxide, UO_2, could dissolve with water and then, the release to the biosphere of fission products and heavier actinides contents in the SNF could occur.[3-5]

This corrosion process is described primarily via the oxidation of U(IV) to U(VI), and then the formation of alteration products, usually containing UO_2^{2+} in their crystal structures:[6]

U(IV) → U (VI) Eq. 1
U(VI) → UO_2^{2+} (s) Eq. 2

Great effort has been performed to study the reaction mechanism and to establish the key parameter that controls the corrosion of the SNF such as a leaching/dissolution experiments[7-9] and the studies of uraninite[10,11] as a natural analogue of the spent nuclear fuel matrix.

These stability studies require the characterization of the products of the SNF and its reaction products, which is a great challenge not only because these materials are very complicated (containing almost the entire periodic table), but also due to its radiotoxicity.[12] The last feature complicates the handling of these substances under security conditions and, therefore, its characterization. The proper characterization technique to analyze these materials should meet various requirements, such as: 1) the samples do not require any special preparation; 2) the technique must allow the analysis of a very small amount of sample and, 3) it must be a non destructive technique.

One technique that meets all the above criteria is Raman spectroscopy.[13] This technique has proven useful in the study of several systems in extreme conditions, such as very high[14] or very low temperatures,[15] high pressures[16] and also radioactivity.[17] The Raman spectroscopy can give information on both the molecular structure and the surrounding environment. However, in order to obtain this information is necessary a precise assignment of the bands in the Raman spectrum and models to interpret the values of the band wavenumbers and changes in these ones. Beside the fact that Raman technique has been already used to analyze the SNF and its alteration products, a database with good assignment of the different bands is still rather limited apart from some works,[7,18-23] and the effort of Frost *et al.*[24-29] who studied a high number of secondary phases. A few research groups[30-32] focused their studies on the characterization of the uranium oxides.

Difficulties in the assignment of the different vibrational bands can be overcome by using theoretical calculations. Solid state codes in modern large computers are nowadays capable of optimizing the structures of complex systems, and then performing theoretical predictions of many observable quantities comparable with experiment.[33-35] *Ab initio* lattice dynamics provide theoretical vibrational spectra as well as

[a] Centro de Investigaciones Energéticas, Medioambientales y Tecnológicas (CIEMAT). Avda/ Complutense, 40– 28040 Madrid– Spain
[b] Instituto de Estructura de la Materia (CSIC). C/ Serrano, 113– 28006 Madrid – Spain.

† Electronic Supplementary Information (ESI) available: Calculated structures of uranium containing minerals using a new pseudopotential; Normal modes of rutherfordine (Pmmn and Imm2 symmetries). See DOI: 10.1039/x0xx00000x

detailed microscopic scale views of the atomic vibrational motion (normal modes), thus allowing a reliable assignment of the experimental Raman bands.[36] One of the methods for which this kind of calculations are feasible is DFT (Density Functional Theory)[37] based on plane waves and employing pseudopotentials.[38] The use of DFPT (Density Functional Perturbation Theory)[36,39,40] has permitted the theoretical prediction of IR and Raman spectra with good level of accuracy and cost/performance ratios. However, its application to minerals containing Rare Earth Elements presents difficulties not only due to the great number of atoms and valence electrons involved, but also to the high level of theory required to describe these elements.[41,42] Uranium is a complex atom showing four oxidation states (+3, +4, +5, and +6) with a very large size of its ions, forming complicated compounds with large coordination numbers. The number of valence electrons in the outer shells, which should be explicitly described, is great and include orbitals of high angular quantum number (5f shell). Good relativistic pseudopotentials needed to describe the inner electrons of these elements suitable for vibrational studies of solids are difficult to find or generate. As a matter of fact, there is very few published work on the theoretical vibrational spectra of uranium containing solids.[43-46] These studies are limited to uranium oxides and nitrides and the unique spectral features considered are the vibrational band wavenumbers. For example, Yun *et al.*[43] determined the phonon spectrum of UO_2 at gamma point and compared the wavenumbers with the experimental ones. Nevertheless, some studies on other properties of these materials[41,42,47-53] and of related gas-phase molecular clusters have been reported.[54-58]

One of the uranyl minerals of interest is the rutherfordine, UO_2CO_3. Rutherfordine is the only known uranyl mineral phase of interest in the SNF that contains only uranyl and carbonate. There are another uranyl carbonate hydrated phases such as blatonite, $UO_2CO_3{\cdot}H_2O$[59] and joliotite, $UO_2CO_3{\cdot}2H_2O$[60] but the structures of both minerals are unknown. Uranium carbonate compounds and their importance in actinide environmental chemistry have been reviewed by Clark *et al.*[61] Carbonate and bicarbonate, present in significant concentrations in many natural waters, are exceptionally strong complexing agents for actinide ions and, therefore, carbonate complexes of actinide ions play an important role in migration from a nuclear waste repository or in accidental site contamination. This is reflected by the formation of many naturally occurring uranyl carbonate minerals such as rutherfordine, liebigite, and andersonite among others.[61] Uranium carbonates may precipitate where evaporation is significant or where the partial pressure of CO_2 is large, rutherfordine becoming a more stable uranium phase with respect to schoepite. Rutherfordine would be expected to replace schoepite in environments where the CO_2 pressure is high, possibly in a repository environment or in saturated soils. Replacement of schoepite by rutherfordine has been observed at the Shinkolobwe U-deposit.[62,63] The study of the structural and thermodynamic stabilities of uranium carbonates is thus particularly relevant to nuclear-waste disposal.

Rutherfordine was discovered by Marckwald[64] and described as a mineral species by Frondel and Meyrowitz.[65] Its solid state structure has been determined from crystals of both the natural mineral and synthetic samples. Rutherfordine forms green-yellow crystals which orthorhombic structure. The structure of rutherfordine was provided by Christ and Clark.[66, 67] The structure was later refined by Finch *et al.*[68]. Christ *et al.*[66] presented two structures: (1) structure A, which is consistent with Pmmn symmetry, and adjacent layers have the CO_3^{2-} groups pointing in opposite directions; and (2) structure B, which is consistent with Imm2 symmetry, and adjacent layers have the CO_3^{2-} groups pointing in the same direction. They suggested that structures A and B are energetically equivalent, and that crystals can contain domains of each structure, separated by stacking faults. Finch *et al.*[68] suggested that structure B should be favored. Pmmn and Imm2 structures are considered in present theoretical calculations, the results indicating that both may be simultaneously present in nature in accordance with the suggestion of Christ *et al.*[66]

In this paper we present a detailed study of the rutherfordine mineral using Raman spectroscopy and DFT calculations. The work is structured as follows: in section 2, the materials and methods used in this work are described for the experimental and theoretical parts of this study. Density functional theory calculations are described as well as the generation of the pseudopotential used for uranium atom. Then, in section 3, experimental results are presented and compared with theoretical data of the Pmmn and Imm2 symmetries and the assignment of main fundamental band wavenumbers is carried out. Moreover, the effect of water addition to the rutherfordine structure is studied by further calculations. Conclusions of this work are presented in section 4.

2 Materials and methods

2.1 Experimental

The analyzed sample is a “uraninite + gummite” mineral from Sierra Albarrana (Córdoba, Spain), collected during the uranium extractive activity in 1960. The sample structure corresponds to the ideal gummite occurrence (central core black and a yellow surrounding zone, formed by several minerals).[10] A detailed description of the mineral setting and other structural characteristics is described elsewhere.[69]

The sample was cut using a diamond saw and polished. A polished section of the sample was analyzed via Raman spectroscopy by using a Horiba LabRam HR evolution spectrometer (Jobin Yvon Technology). A red laser of HeNe with a wavelength of 632.81 nm and an operation power of 20mW was used as excitation source. The laser was focused onto the sample using the 100x objective of the confocal microscope BX4 with confocal 800mm; the scattered light was collected with the same objective and then dispersed with a Jobin-Yvon spectrometer (600 grooves / mm), and detected with a Peltier cooled CCD detector (256 x 1024 pix.). The spectral resolution was about 1 cm^{-1} per pixel.

2.2 Theoretical

Rutherfordine unit cell has been modeled using the CASTEP code,[33] a module of the Materials Studio package.[70] The generalized gradient approximation (GGA) with several different energy functionals was employed. The main one was PBESOL functional.[71,72] Also, since rutherfordine structure is composed of sheets held together by van der Waals forces, we used the PBE functional[71] with Grimme empirical dispersion correction, the DFT-D2 approach,[73] to evaluate the importance of this kind of interactions.

Geometry optimization was carried out using the Broyden–Fletcher–Goldfarb–Shanno optimization scheme[74] with a convergence threshold on atomic forces of 0.01 eV/Å. The different kinetic energy cutoffs and k-point meshes[75] adopted will be indicated in each case. They must be selected to ensure good convergence for computed structures and energies.

For the calculations of vibrational properties, the linear response density functional perturbation theory (DFPT)[36,39,40] implemented in the CASTEP code was used, where the phonon wavenumbers at the gamma point of the Brillouin zone were computed using atomic displacement perturbations. Raman intensities are third-order derivatives of total energy with respect to vibrational mode (atomic position) and laser field (electric field, twice). These are calculated in CASTEP[34] using a combination of perturbation theory (second derivative with respect to field) and finite differences (third derivative with respect to atomic displacement). The wavenumbers presented in this work have not been scaled to correct for anharmonicity and correspond to the harmonic approximation of the force field.

Since the CASTEP code only allows determining vibrational properties using norm conserving pseudopotentials and there is not such a pseudopotential for uranium atom, we decided to construct a new one. First, we generated a Troullier-Martins type norm-conserving pseudopotential[76] using program fhi98PP[77] in cpi format. The pseudopotential included relativistic effects (scalar relativistic all electron calculations are used) and it was generated using the GGA-PBE[71] method. The electronic configuration of atomic uranium is $6s^2 6p^6 6d^1 5f^3 7s^2$. The pseudopotential has been obtained from an ionized electronic configuration $6s^2 6p^6 6d^1 5f^3 7s^0$ with cutoff radii equal to 1.236, 2.447, 2.166 and 2.447 for *s*, *p*, *d*, and *f* angular momentum, respectively. The s component of the pseudopotential has been chosen as the local potential, and a Kleinman-Bylander form[78] has been used. Then, we transformed it into recpot format used in CASTEP by using the tool cpi2recpot.[79] The use of this pseudopotential implies that 14 valence electrons must be treated explicitly. In other works, 32 electrons were included in the valence shell.[56] This further increases the computational cost and only marginally improves the performance.[42,57]

This pseudopotential reproduces accurately the all-electron calculation in the reference configuration in which it was generated. Further, checks of the smoothness of the nodeless pseudo-wave-functions near the cutoff radii, continuity of the logarithmic energy derivatives and transferability of the pseudopotential were performed. In order to probe the generated norm-conserving pseudopotential under different environments and to validate it, we have computed the structures of a series of uranium containing minerals with small cutoffs and K meshes. The results are given in a table in Appendix A of Supplementary information. As can be seen in Table A.1 the results are quite good for the lattice parameters of the species involved. Better results are expected upon increasing the cutoff values and using larger K meshes.

3 Results and discussion

3.1 Structure

A determination of the best geometrical structure was first carried out searching for a minimum in the potential energy surface. From the optimized structure we have obtained both the structural parameters and the X-ray powder pattern.

We have considered both orthorhombic (Z=2) structures in rutherfordine, Pmmn and Imm2. The results are nearly the same and the energy difference for the optimized structures is less than 0.001 eV, the Pmmn structure being the lowest one.

The structure of rutherfordine contains approximately linear UO_2^{2+} uranyl ions that are coordinated by six O atoms arranged at the equatorial vertices of uranyl hexagonal bipyramids. These O atoms belong to four carbonate ligands and U is bonded with two carbonate ions in a bidentate manner and two in a monodentate manner. Each uranyl polyhedron is linked to two other uranyl polyhedra in a *trans* arrangement by edge sharing, resulting in chains of polyhedra. Adjacent chains are linked by the sharing of equatorial vertices between uranyl polyhedra, which results in a sheet structure that contains triangular voids. Carbonate triangles occupy one half of the voids, such that they share the equatorial edges of two adjacent uranyl hexagonal bipyramids and single vertices of two additional uranyl polyhedra (see Fig. 1). The resulting sheets or layers are electroneutral, and adjacent sheets in rutherfordine are bonded together by van der Waals forces. The UO_2CO_3 layers are staggered with respect to the layer above or below, such that uranyl units lie above and below a carbonate carbon atom in adjacent layers. Layers are separated by a distance of about 4.6 Å. The structure is shown in Fig. 1. Figures 1.a and 1.b show two contiguous sheets (Pmmn and Imm2 symmetry structures). In Fig. 1.c. a view from (010) axis is observed (similar for the two symmetry structures), showing the relative disposition of the uranyl polyedra and carbonate triangles in the plane. As can be seen, for the Pmmn structure the carbonate triangles in contiguous sheets point in opposite directions while in the Imm2 structure they point in the same direction.

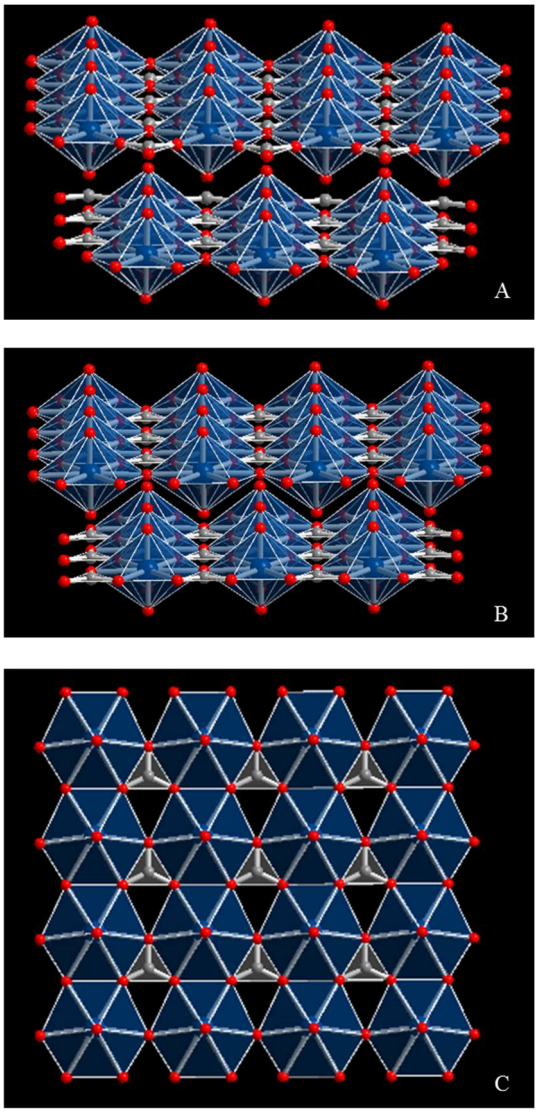

Fig. 1 a) Two contiguous sheets in the structure of rutherfordine for the Pmmn structure; b) as Fig. 1.a. for the Imm2 structure; c) upper (010) view of a sheet in the structure of rutherfordine. Color code: U-Blue, O-Red, C-Carbon.

The lattice parameters of rutherfordine, as well as the volumes and densities, were determined in calculations with increasing complexity by increasing the different parameters (larger kinetic energy cutoffs and K meshes). The optimizations performed with a cutoff of 1000 eV and a K mesh of 5 x 3 x 6 (18 Kpoints) gave well converged structures and were considered sufficient to determine the final material properties. Table 1 gives the final lattice parameters, volumes and densities obtained for the Pmmn and Imm2 structures, respectively. Tables 2 and 3 give the corresponding bond distances and angles.

Table 1 Lattice parameters.

Calculation.	a (Å)	b (Å)	c (Å)	α	β	γ	Vol. (Å^3)	Dens. (g/cc)
Pmmn	4.8257	9.3321	4.2720	90	90	90	192.4	5.697
Imm2	4.8267	9.3639	4.2727	90	90	90	193.1	5.675
Exp.[68]	4.840	9.273	4.298	90	90	90	192.9	5.682

Table 2 Bond distances (in Å).

Bond	Exp.[68]	Pmmn	Imm2
U-O3	2.444	2.435	2.428
U-O2	2.48	2.436	2.437
U-O2'	2.52	2.525	2.535
U-O1	1.744	1.764	1.764
U-C	2.94	2.912	2.918
C-O3	1.32	1.301	1.301
C-O2	1.26	1.280	1.280
<CO>	1.28	1.287	1.287
C-O1	2.93	2.946	2.960

Table 3 Bond angles (in deg).

Bond angle	Exp.[68]	Pmmn	Imm2
O1a-U-O1	179	178.61	179.92
O1-U-O2 x4	91	90.59	90.03
O1-U-O2b x4	89	89.40	89.97
O1-U-O3 x4	90.1	89.91	89.99
O2-U-O2c	60.8	59.89	58.70
O2b-U-O2d	62.1	62.32	62.61
O3-U-O2b x2	67.0	66.62	66.72
O3-U-O2 x2	51.6	52.27	52.13
O2-C-O2e	131	128.42	128.33
O2-C-O3 x2	114	115.79	115.83
<O-C-O>	120	120	120

The powder X-ray pattern of rutherfordine was computed[80] from the experimental[68] and computed structures using CuK_α radiation (λ=1.540598 Å). The most intense lines (I > 10%) are compared in Figures 2.b, 2.c, and 2.d, and, as can be seen, the line positions and intensities are in good agreement. The use of spectra derived directly from the experimental and computed structures allows for a fair comparison of the results free of interferences as the experimental conditions or possible artifacts as the presence of sample impurities since both are determined under identical conditions. Nevertheless, the use of an experimental pattern also leads to an excellent agreement. Computer program XPowder[81] using the PDF-2 database[82] directly recognizes the computed spectrum as that of rutherfordine mineral (pattern 89-6527).[68] The experimental X-ray spectrum can be seen in Fig. 2.a where it is compared with the previously described spectra. The precise values of the main reflections for the Imm2 and Pmmn computed structures and the experimental ones are given in Table 4.

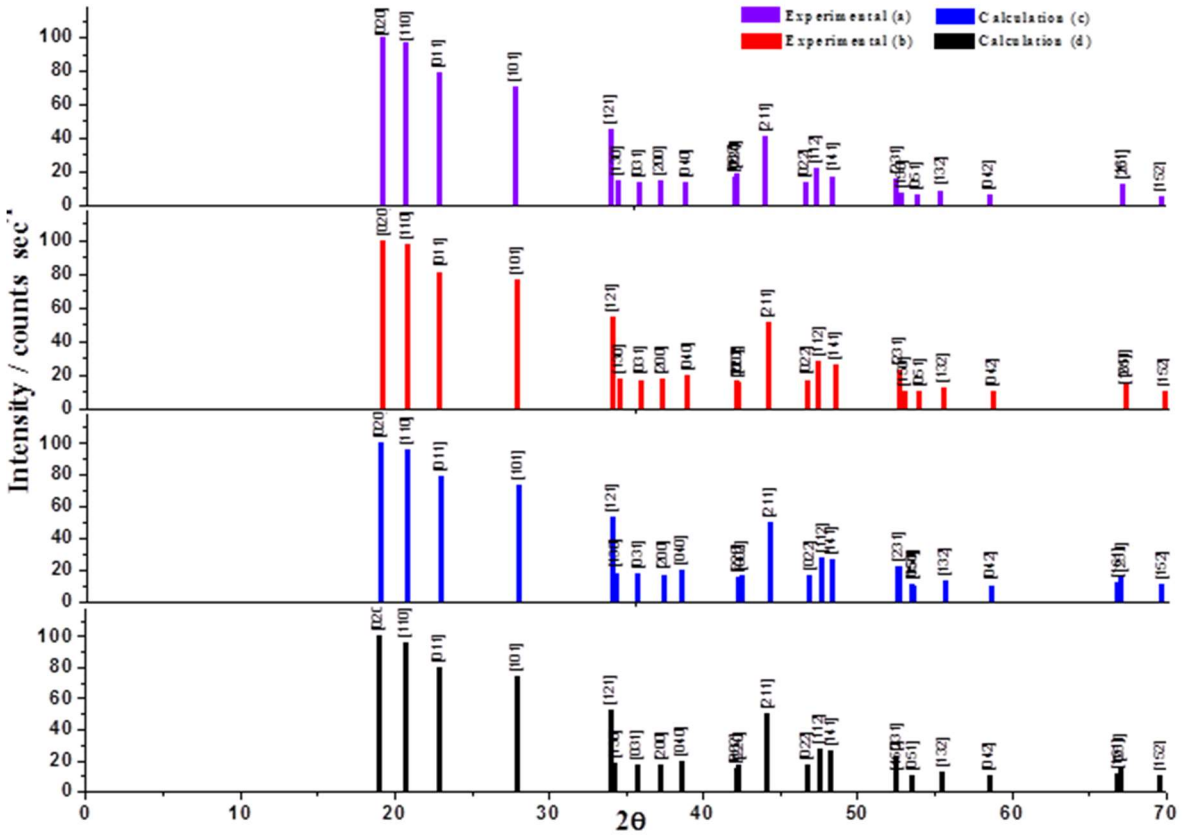

Fig. 2 X-ray powder spectrum of rutherfordine using CuK_{α} radiation: a) Experimental spectrum (pattern 89-6527 in the PDF-2 database[68]) b) X-ray powder spectrum computed form experimental geometry; c) X-ray powder spectrum computed from calculated geometry (Pmmn); c) X-ray powder spectrum computed from calculated geometry (Imm2).

Table 4 Main reflections in the X-ray powder spectrum of Rutherfordine. The experimental data are from the pattern 89-6527 in the PDF-2 database.[68]

Experimental reflections				Calculated reflections Pmmn			Calculated reflections Imm2		
2Θ	d(Å)	I (%)	hkl	2Θ	d(Å)	I (%)	2Θ	d(Å)	I (%)
19.127	4.636	100.0	020	19.004	4.6660	100.0	18.939	4.682	100.0
20.684	4.290	97.397	110	20.705	4.2865	96.227	20.687	4.290	95.591
22.786	3.899	78.679	011	22.876	3.8846	79.564	22.859	3.887	79.089
27.736	3.214	70.771	101	27.870	3.1987	73.600	27.864	3.199	73.535
33.912	2.641	45.445	121	33.952	2.6383	52.598	33.909	2.641	52.942
34.398	2.605	14.514	130	34.269	2.6146	18.163	34.182	2.621	18.049
35.752	2.509	12.913	031	35.675	2.5147	17.219	35.591	2.520	17.129
37.121	2.420	14.615	200	37.235	2.4128	17.005	37.227	2.413	16.853
38.814	2.318	13.213	040	38.558	2.3330	19.736	38.422	2.341	19.670
42.010	2.149	16.216	002	42.128	2.1433	14.949	42.269	2.136	16.452
42.084	2.145	18.218	220	42.277	2.1360	16.627	42.089	2.145	14.870
44.001	2.056	40.741	211	44.151	2.0496	50.157	44.134	2.050	49.782
46.541	1.950	12.913	022	46.734	1.9422	16.829	46.697	1.944	16.699
47.268	1.921	21.521	112	47.522	1.9118	27.663	47.505	1.912	27.535
48.373	1.880	17.017	141	48.242	1.8849	25.788	48.125	1.889	25.791
52.489	1.742	15.315	231	52.519	1.7410	22.368	52.451	1.743	22.219

3.2 Raman spectra and band assignment

In this section we analyze the experimental profile of the rutherfordine Raman spectra obtaining the wavenumber of the main characteristic bands. Also the theoretical spectrum is presented and the assignment of the vibrational bands is performed. The results are compared with some published data of this mineral phase.

In order to calculate the number of contributions of a given band from the experimental spectrum we carry out the analysis by the second derivate method.[83] The first derivative gives us an idea of the number of contributions involved but, as usual in spectroscopy, is the second derivative which enables us to determine the number of contributions, since each one leads to a minimum.

The Raman spectra for the Pmmn and Imm2 structures were computed at T=298 K, λ=532 nm, FWHM=5 cm^{-1}. The atomic motions associated to each vibrational normal mode are shown in the supplementary information (Appendix B and C). Fig. 3 shows the experimental Raman spectrum of rutherfordine, together with the calculated ones. A summary of the measured and calculated spectra is shown in Tables 5 and 6 for Pmmn and Imm2, respectively, as well as the approximate assignments of the vibrational modes, derived from the calculations. As can be seen in Fig. 3, the general aspect of the computed spectrum is very similar to that of the experimental spectrum up to 1550 cm^{-1}. The band observed at higher wavenumber (~ 1603 cm^{-1}) in the experimental spectrum does not appear in the computed ones, as expected, due to the fact that this band corresponds to the water bending vibration, and the calculations do not include water within the structure. A more detailed comparison will be given below. Note that when the symmetry of a certain vibration is cited, we refer to that of the Pmmn structure. To find the corresponding symmetry for Imm2 structure, see Table 6 given below.

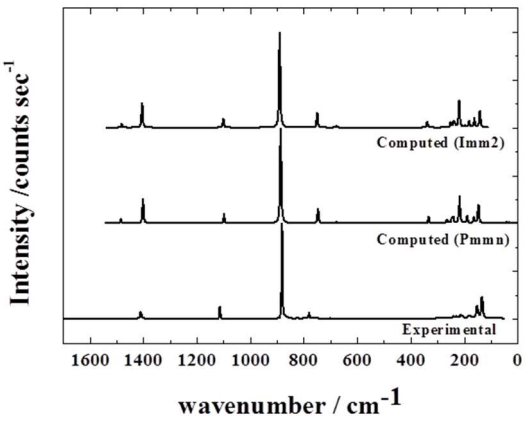

Fig. 3 Calculated and experimental Raman spectra.

Table 5 Experimental and calculated Raman shifts, calculated intensities and assignments (Pmmn symmetry).

Exp. Raman shift (cm^{-1})	Calc. Raman shift (cm^{-1})	Irr. Rep. (D_{2h})	Intensity (Å^4)	Assignment
78.63	32.743	A_g	0.051	$T(UO_2^{2+}+CO_3^{2-})$
95.34	43.405	B_{3g}	0.129	$T(UO_2^{2+}+CO_3^{2-})$
133.77	147.179	B_{1g}	11.632	$\delta^a(UO_2^{2+})+\delta^{op}(CO_3^{2-})$
152.91	149.758	B_{3g}	2.860	$\delta^{op}(CO_3^{2-})$
168.187	164.700	B_{3g}	4.693	$T(CO_3^{2-})$
187.24	189.777	B_{3g}	8.011	$\delta^a(UO_2^{2+})$
212.98	217.417	A_g	35.316	$T(CO_3^{2-})$
241.59	241.484	B_{2g}	7.366	$\delta^s(UO_2^{2+})+\delta^{ip}(CO_3^{2-})$
256.68	264.646	B_{2g}	7.636	$\delta^s(UO_2^{2+})+\delta^{ip}(CO_3^{2-})$
339.15	332.824	B_{2g}	16.935	$\delta^{ip}(CO_3^{2-})$
700.29	677.803	A_g	15.199	$\delta^{ip}(CO_3^{2-})$
754.448	752.046	B_{3g}	0.432	$\delta^{op}(CO_3^{2-})$
780.203	746.833	B_{2g}	110.074	$\delta^{ip}(CO_3^{2-})$
793.045	-	-	-	-
803.534	-	-	-	-
823.306	-	-	-	-
882.288	886.469	A_g	879.905	$v^s(UO_2^{2+})$
1113.33	1097.712	A_g	120.246	$v^s(CO_3^{2-})$
1408.98	1401.211	A_g	407.713	$v^a(CO_3^{2-})$
1498.92	1482.837	B_{2g}	76.985	$v^a(CO_3^{2-})$

Table 6. Experimental and calculated Raman shifts, calculated intensities and assignment (Imm2 symmetry).

Exp. Raman shift (cm^{-1})	Calc. Raman shift (cm^{-1})	Irr. Rep. (D_{2h})	Intensity (Å^4)	Assignation
78.63	-	-	-	-
95.34	-	-	-	-
133.77	141.673	A_2	10.780	$\delta^a(UO_2^{2+})+\delta^{op}(CO_3^{2-})$
152.91	-	-	-	-
168.187	162.271	B_1	7.754	$\delta^a(UO_2^{2+})+\delta^{op}(CO_3^{2-})$
187.24	182.062	B_1	6.165	$\delta^a(UO_2^{2+})+\delta^{op}(CO_3^{2-})$
212.98	218.675	A_1	34.726	$\delta^s(UO_2^{2+})+T(CO_3^{2-})$
241.59	239.638	B_2	6.546	$\delta^s(UO_2^{2+})+\delta^{ip}(CO_3^{2-})$
256.68	250.776	B_2	8.407	$\delta^s(UO_2^{2+})+\delta^{ip}(CO_3^{2-})$
339.15	338.196	B_2	17.723	$\delta^{ip}(CO_3^{2-})$
700.29	677.882	A_1	16.450	$\delta^{ip}(CO_3^{2-})$
754.448	750.148	B_1	0.542	$\delta^{op}(CO_3^{2-})$
780.203	749.753	B_2	112.461	$\delta^{ip}(CO_3^{2-})$
793.045	-	-	-	-
803.534	-	-	-	-
823.306	-	-	-	-

882.288	889.836	A_1	872.824	$\nu^s(UO_2^{2+})$
1113.33	1099.867	A_1	117.486	$\nu^s(CO_3^{2-})$
1408.98	1403.178	A_1	407.867	$\nu^a(CO_3^{2-})$
1498.92	1480.873	B_2	75.720	$\nu^a(CO_3^{2-})$

The Raman spectra of the regions 1200-850 cm^{-1} and 1700-1200 cm^{-1} are shown in Figures 4.a and 4.b, respectively, together with the computed spectra.

Fig. 4.a shows the region of the uranyl stretching vibration. In this region it can be observed a main band at 882 cm^{-1} which corresponds to the uranyl symmetric stretching vibration ν_1, which is commonly used as a fingerprint of this mineral.[69] The value was very well reproduced by the theoretical calculations (886 cm^{-1} and 900 cm^{-1}, for Pmmn and Imm2, respectively, A_g symmetry), and it is in agreement with previous published data (886 cm^{-1}).[25] At higher wavenumbers (around 1113 cm^{-1}) we found a band which is assigned to the CO_3^{2-} symmetric stretching vibration ν_1 (free CO_3^{2-} ion value of 1060 cm^{-1}), which is also in good agreement with both the calculated value (1098 cm^{-1} and 1100 cm^{-1}, A_g symmetry) and the experimental value of ref.[25] (1115 cm^{-1}).

Fig. 4.b shows the spectrum in region 1700-1200 cm^{-1}. The band at 1409 cm^{-1} is assigned to the asymmetric stretching vibrations of CO_3^{2-} ion ν_3 and this value is very close to the computed wavenumbers (1401 cm^{-1} and 1403 cm^{-1}). Frost *et al.*[25] observed this band at 1412 cm^{-1}.

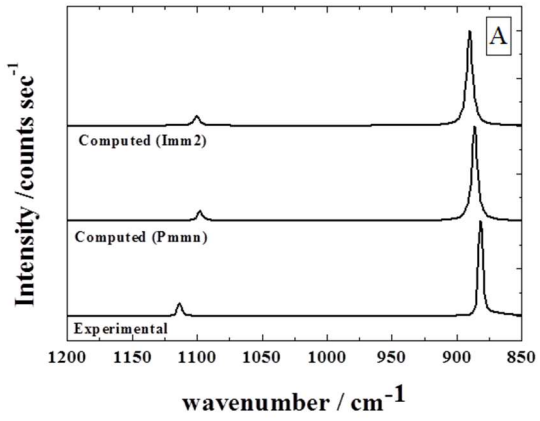

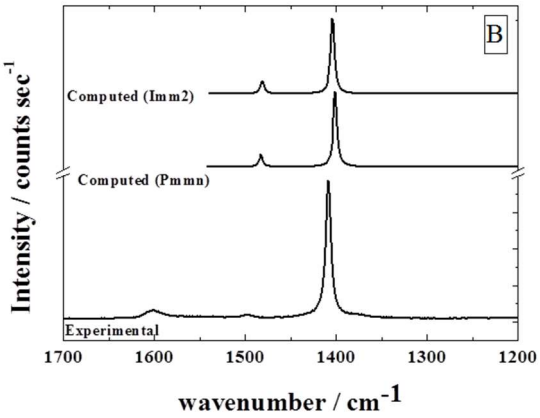

Fig. 4 a) Raman spectrum of the region 850-1200 cm^{-1}; b) Raman spectrum of the region 1200-1700 cm^{-1}.

The existence of a less intense band at about 1499 cm^{-1} can be explained as a result of the splitting of the ν_3 band. In the free undistorted ion it is degenerate, symmetry E', and located at about 1415 cm^{-1}. The band is splitted into two components when the ion symmetry is lowered from D_{3h} to C_{2v}, whose computed values are 1401 and 1483 cm^{-1} with symmetries A_g and B_{2g}, respectively, for the Pmmn structure and 1403 and 1481 cm^{-1} for Imm2 structure. The experimental value of the splitting is Δ=1499-1409=90 cm^{-1} while the computed values are 82 and 78 cm^{-1}. The values are also comparable to the IR spectrum bands at[84] 1414 and 1505 cm^{-1} or[85] 1433 and 1520 cm^{-1}.

The Raman spectra of the regions 500-0 cm^{-1} and 850-500 cm^{-1} are shown in Figures 5.a and 5.b, respectively, together with the computed spectra.

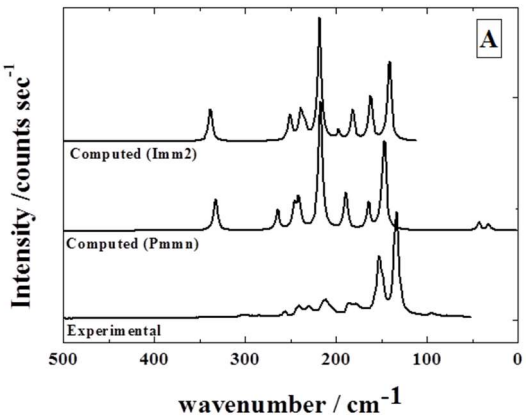

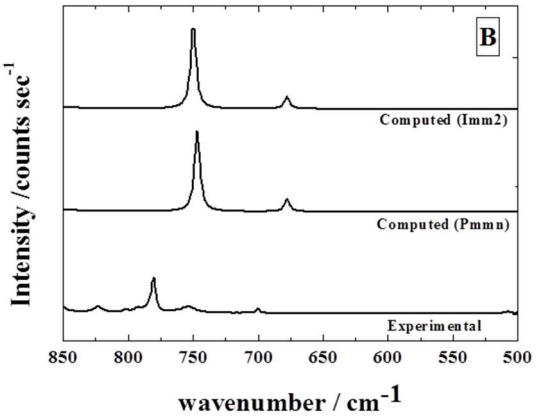

Fig. 5 a) Raman spectrum of the region 0-500 cm^{-1}; b) Raman spectrum of the region 500-850 cm^{-1}.

The low wavenumber region 500-0 cm^{-1} is shown in Fig. 5.a. The bands located at 339, 257, 242, 213, 187, 168, 153, and 134 cm^{-1} have theoretical counterparts of 332, 265, 242, 217, 190, 165, 150, and 147 cm^{-1} for Pmmn and 338, 251, 240, 219, 182, 162 and 142 cm^{-1}, for the Imm2 symmetry. The first one, at 339 cm^{-1}, is assigned to a carbonate in plane bending vibration (B_{2g}), and that located at 153 cm^{-1} to a carbonate out of plane vibration (B_{3g}). While the 257 and 242 cm^{-1} bands are assigned mainly to uranyl symmetric bending vibrations (B_{2g}), the 187 and 134 cm^{-1} bands are assigned to uranyl antisymmetric bending vibrations (B_{3g} and B_{1g}). Finally, the 213 and 168 cm^{-1} bands are assigned to carbonate group translations (A_g and B_{3g}). The latest bands found at 95 and 79 cm^{-1} are not as well reproduced theoretically and may be described as overall carbonate and uranyl group translations.

Among the low wavenumber bands of the published data[25] a band is found at 343 cm^{-1} which seems to split into two components at 336 and 330 cm^{-1}. These bands were attributed to the ν(U–Oequatorial) vibrations.[86] As can be seen in the vibrational mode picture, the calculated band at 333 cm^{-1} (associated to the experimental value of 339 cm^{-1}), actually represents a carbonate in plane vibration. Bands were also observed at 279, 263, 252 and 241 cm^{-1} (bands at 257 and 242 cm^{-1} appear in our spectrum) and were ascribed without specification to the v_2 bending modes of the $(UO_2)^{2+}$ units and lattice vibrations. We believe that they correspond to uranyl symmetric bending vibrations, the antisymmetric ones and lattice vibrations falling somewhat lower in wavenumber.

Fig. 5.b shows the region 850-500 cm^{-1}. The bands at 700 and 780 cm^{-1} are attributed to the CO_3^{2-} in plane bending vibrations v_4 and are calculated at 678, and 747 cm^{-1}, for Pmmn and 678 and 750 cm^{-1} for Imm2. The free ion wavenumber value is 680 cm^{-1}. This vibration (E'' symmetry) splits, as the v_3 one, into two components of symmetries A_g and B_{2g}. In this case the second one has the largest intensity. The splitting is Δ=69 cm^{-1} for Pmmn and 72 cm^{-1} for Imm2 while the experimental value is 80 cm^{-1}. The CO_3^{2-} out of plane deformation vibration v_2 is believed to fall at 754 cm^{-1} while the theoretical value is 752 cm^{-1} for Pmmn and 750 cm^{-1} for Imm2 as can be seen in the vibrational mode pictures (see Fig. B.1 in Appendix B and Fig. C.1 in Appendix C of Supplementary information). The free ion value is however 880 cm^{-1}. It is very weak in the theoretical Raman spectra as expected from an inactive Raman vibration for the free carbonate ion.

It should be noted that weak bands at 793, 803, and 823 cm^{-1} do not have counterparts in the theoretical spectra; these bands must correspond to other species of carbonate anions in the rutherfordine structure[25,85] or other different mineral phases present in the natural sample being studied.

Raman spectra of schoepite,[28] shows bands at 897, 886, 870, 855, 839, 826, 817, 802, 554, 545, 507, 460, 458, 402, 351, 330, 305, 274, 248, 216, 194 and 168 cm^{-1}. The bands at 803 and 823 cm^{-1} are close to those schoepite bands at 802 and 826 cm^{-1}. Thus, it may be relics of schoepite bands. They were attributed[28] to the splitting of $v^s(UO_2^{2+})$ symmetric stretching vibration in schoepite (different U–O bond lengths in uranyl) or to ν(U–OH) bending vibrations. This correspondence is in accordance with the solid solution suggestion, which implies that solid solutions with limited solubility may exist in the system $UO_2(CO_3)/UO_2(OH)_2{\cdot}yH_2O$ (rutherfordine/schoepite, metaschoepite, and dehydrated schoepite), thus forming $UO_2(CO_3)_{1-x}(OH)_{2x}{\cdot}yH_2O$.[25, 68, 84, 87]

The band at 793 cm^{-1} can also be related to the uranophane alpha band found[26,69] at about 797 cm^{-1}.

From the analysis above described, it can be concluded that both theoretical spectra corresponding to the Pmmn and Imm2 symmetries are similar to the experimental one. However, in the Raman spectra associated to the Pmmn structure we note the presence of three additional active translation modes, absent in the calculated Raman spectrum associated to the Imm2 structure. Nonetheless, both structures may be simultaneously present in nature, as suggested by Christ *et al.*[66]

3.3 Effects of the introduction of dispersion corrections and water molecules in the structure of rutherfordine

Additional calculations were carried out with the aim of: a) analyzing the influence of dispersion corrections in the theoretical results and, b) studying the influence of the introduction of water molecules inside the structure of rutherfordine in the band wavenumbers, particularly in the out of plane deformation wavenumber for the carbonate groups. A comparison of this wavenumber was also carried out with values reported in the literature.

Since the sheets in the structure of rutherfordine are bonded together by van der Waals forces, we have carried out calculations using the PBE functional[71] including the empirical dispersion correction of Grimme.[73] The kinetic energy cutoff used was 1200 eV and the K mesh 5 x 3 x 6 (18 K points). The computed lattice parameters were a=4.8647 Å, b=9.5435 Å, c= 4.3295 Å (α=β=γ=90 deg). The main effect is, therefore, the increase of the intersheet distance (b parameter). The agreement with experimental structure is worse than in the calculations obtained in previous sections and thus, the PBESOL[72] functional works better in this case, at least for the

structural determination. The vibrational Raman spectra is however quite similar to the PBESOL one. Dispersion corrections, therefore, do not seem to modify significantly the calculated spectra.

As mentioned before, the computed spectra do not include water molecules in the rutherfordine structure and since the presence of water might cause significant shifts in the bands associated with both UO_2^{2+} and CO_3^{2-} units, additional calculations were carried out. Particularly, the carbonate out of plane deformation wavenumber was shown to be much lower than the free ion value. The main displacements in this mode arise from the carbon atoms of the carbonate groups. Due to the presence of uranyl groups placed just above and below them, the out of plane motion may be hindered and water molecules placed in the intersheet space could modify the corresponding wavenumber. Two water molecules were introduced in the space between the sheets of the unit cell of rutherfordine. The calculation was performed again with the dispersion corrected PBE functional, a kinetic energy cutoff of 900 eV and a 3 x 1 x 3 K mesh (5 K points). The intersheet space was greatly increased, but the carbonate main bands were only slightly modified: $\nu^a(CO_3^{2-})$=1473, 1378; $\nu^s(CO_3^{2})$=1091; $\delta^{op}(CO_3^{2-})$=761; $\delta^{ip}(CO_3^{2-})$=750, 680.
Majumdar *et al.*[58] carried out molecular calculations (gas phase) of UO_2CO_3, PuO_2CO_3, and related clusters including hydrated species using DFT (B3LYP functional), second-order Moller-Plesset (MP2) perturbation and multireference configuration interaction methods and large gaussian basis sets. The calculated ν_2 and ν_4 vibrational wavenumbers of the carbonate group were given only for the isostructural PuO_2CO_3 gas phase species. The values obtained at the MP2 level for the anhydrous system PuO_2CO_3 are ν_2=(629,719) cm^{-1} and ν_4=754 cm^{-1}. The ν_4 value obtained for the anhydrous species, 754 cm^{-1}, is thus consistent with our calculated wavenumber of 752 cm^{-1} and present experimental value of 754 cm^{-1}.

4 Conclusions

A natural rutherfordine mineral was characterized by means of Raman spectroscopy combined with theoretical calculations based on DFT methods. The structural parameters and X-ray powder spectrum obtained indicates that the rutherfordine mineral is accurately described by our theoretical computations. Pmmn and Imm2 structures were considered in this work. Since these structures are nearly degenerate and the properties computed from them are very similar, we conclude that both may simultaneously be present in nature in accordance with the suggestion of Christ et al.[66]

The Raman spectrum obtained experimentally is also fairly well reproduced. Main vibrations used as a fingerprint to identify rutherfordine are the two ν_1 symmetric stretching bands of the UO_2^{2+} and CO_3^{2-} groups placed at 882 and 1113 cm^{-1}, respectively. These bands are very well reproduced theoretically at 886 and 1098 cm^{-1}, respectively. Next bands, obtained by Raman spectroscopy, located at 1409 and 780 cm^{-1}, are attributable to the CO_3^{2-} group asymmetric stretching and in plane bending modes ν_3 and ν_2, the calculated ones being located at 1401 and 747 cm^{-1}. In the low wavenumber region, we found three main bands at 134, 153 and 213 cm^{-1}, which are well reproduced by theoretical calculations with wavenumbers located at 147, 150 and 217 cm^{-1}.

For most of the bands in the experimental spectrum we found a correspondence to bands in the theoretical one and, therefore, they were assigned to specific vibrational motions. The band wavenumbers which are not reproduced in our theoretical calculations were attributed to the presence of other uranyl minerals as uranophane.

The introduction of dispersion corrections and the introduction of water molecules into the space between the sheets of the unit cell of rutherfordine do not modify the computed Raman spectrum significantly.

Acknowledgements

This work was supported by ENRESA in the project: Nº 079000189 “Aplicación de técnicas de caracterización en el estudio de la estabilidad del combustible nuclear irradiado en condiciones de almacenamiento” (ACESCO) and project FIS2013-48087-C2-1-P. Supercomputer time by the CETA-CIEMAT and CESGA centers are also acknowledged. This work has been carried out in the context of a CSIC – CIEMAT collaboration agreement: “Caracterización experimental y teórica de fases secundarias y óxidos de uranio formados en condiciones de almacenamiento de combustible nuclear”.

References

1 SKB-91, *Final Disposal of spent nuclear fuel. Importance of the bedrock for safety. Report 92-20. May*, 1992.
2 R. C. Ewing, *Nat. Mater.*, 2015, **14**, 252.
3 D. W. Shoesmith, *J. Nucl. Mater.*, 2000, **282**, 1.
4 S. Sunder, *Nucl. Technol.,* 1998, **122**(2), 211.
5 H. Christensen and S. Sunder, *J. Nucl. Mater.*, 1996, **238**(1), 70.
6 O. Roth and M. Jonsson, *Cent. Eur. J. Chem.,* 2008, **6**(1), 1.
7 M. Amme, B. Renker, B. Schmid, M. P. Feth, H. Bertagnolli and W. Döbelin, *J. Nucl. Mater.*, 2002, **306**(2-3), 202.
8 A. Rey, J. Giménez, I. Casas, F. Clarens and J. de Pablo, *Appl. Geochem.*, 2008, **23**(8), 2249.
9 C. M. Lousada, M. Trummer and M. Jonsson, *J. Nucl. Mater.*, 2013, **434**(1-3), 434.
10 C. Frondel, *Am. Mineral.*, 1956, **41**, 539.
11 J. Plášil, *J. Geosci.*, 2014, **59**, 99.
12 J. Bruno and R. C. Ewing, *Elements*, 2006, **2**(6), 343.
13 J. Dubessy, M. C. Caumon and F. Rull (Editors), *Raman spectroscopy applied to Earth sciences and cultural heritage*, European Mineralogical Union, 2011.
14 J. M. Chalmers and P. R. Griffiths (Editors), *Handbook of Vibrational Spectroscopy: Vibrational Raman Spectroscopy of High-temperature Superconductors*, John Wiley & Sons Ltd, 2002.

15 V. Muñoz-Iglesias, O. Prieto-Ballesteros and L. J. Bonales, *Geochim. Cosmochim. Acta*, 2014, **125**, 466.

16 A. Arencibia, M. Taravillo, F. J. Pérez, J. Núñez and V. G. Baonza, *Phys. Rev. Lett.*, 2002, **89(19)**, 195504.

17 G. Guimbretiere, L. Desgranges, C. Jegou, A. Canizares, P. Simon, R. Caraballo, N. Raimboux, M. F. Barthe, M. R. Ammar, O. A. Maslova, F. Duval and R. Omnee, *IEEE Trans. Nucl. Sci.*, 2014, **61**, 2045.

18 R. Sobry, *J. Inorg. Nucl. Chem.*, 1973, **35**(8), 2753.

19 L. Maya and G. M. Begun, *J. Inorg. Nucl. Chem.*, 1981, **43(11)**, 2827.

20 B. M. Biwer, W. L. Ebert and J. K. Bates, *J. Nucl. Mater.*, 1990, **175**(3), 188.

21 a) E. Faulques, R. E. Russo and D. L. Perry, *Spectrochim. Acta, Part A*, 1993, **49**(7), 975.; b) E. Faulques, R. E. Russo and D. L. Perry, *Spectrochim. Acta, Part A*, 1994, **50**(4), 757.; c) E. Faulkes, F. Massuyeau, N. Kalashnyk and D. L. Perry, *Spectrosc. Eur.,* 2015, **27**, 14.

22 S. Bastians, G. Crump, W. P. Griffith and R. Withnall, *J. Raman Spectrosc.*, 2004, **35**(8-9), 726.

23 R. J. P. Driscoll, D. Wolverson, J. M. Mitchels, J. M. Skelton, S. C. Parker, M. Molinari, I. Khan, D. Geeson and G. C. Allen, *RSC Adv.*, 2014, **4**, 59137.

24 R. L. Frost and J. Čejka, *J. Raman Spectrosc.*,200, **38**(11), 1488.

25 R. L. Frost and J. Čejka, *J. Raman Spectrosc.*, 2009, **40**(9), 1096.

26 R. L. Frost, J. Čejka, M. L. Weier and W. Martens, *J. Raman Spectrosc.*, 2006, **37**(4), 538.

27 R. L. Frost, J. Čejka, M. L. Weier and W. Martens, *Spectrochim. Acta, Part A,* 2006, **63**, 305.

28 R. L. Frost, J. Čejka and M. L. Weier, *J. Raman Spectrosc.*, 2007, **38**(4), 460.

29 R. L. Frost, M. J. Dickfos and J. Čejka, J. *Raman Spectrosc.*, 2008, **39**(5), 582.

30 H. He and D. Shoesmith, *Phys. Chem. Chem. Phys.*, 2010, **12**, 8109.

31 L. Desgranges, G. Baldinozzi, P. Simon, G. Guimbretière and A. Canizares, *J. Raman Spectrosc.*, 2012, **43**(3), 455.

32 D. Manara and B. Renker, *J. Nucl. Mater.*, 2003, **321**(2-3), 233.

33 S. J. Clark, M. D. Segall, C. J. Pickard, P. J. Hasnip, M. I. J. Probert, K. Refson and M. C. Payne, *Zeitschrift für Kristallographie*, 2005, **220**, 567.

34 V. Milman, K. Refson, S. J. Clark, C. J. Pickard, J. R. Yates, S. P. Gao, P. J. Hasnip, M. I. J. Probert, A. Perlov and M. D. Segall, *J. Mol. Struct.: THEOCHEM*, 2010, **954**(1-3), 22.

35 a) X. Gonze, G.-M. Rignanese, M. Verstraetre, J.-M. Beuken, R. Pouillon and R. Caracas, *Zeitschrift für Kristallographie*, 2005, **220**, 558; b) P. Giannozzi, S. Baroni, N. Bonini, M. Calandra, R. Car, C. Cavazzoni, et al., *J. Phys.: Condens. Matter*, 2009, **21**(39), 395502.; c) F. Pascale, C. M. Zicovich-Wilson, F. López Gejo, B. Civalleri, R. Orlando and R. Dovesi, *J. Comput. Chem.*, 2004, **25**(6), 888.; d) E. Artacho, E. Anglada, O. Diéguez, J. D. Gale, A. García, J. Junquera, R. M. Martin, P. Ordejón, J. M. Pruneda, D. Sánchez-Portal and J. M. Soler, *J. Phys.: Condens. Matter*, 2008, **20**(6), 064208.

36 K. Refson, P. R. Tulip and S. J. Clark, *Phys. Rev. B*, 2006, **73(15)**, 155114.

37 a) P. Hohenberg and W. Kohn, *Phys. Rev.*, 1964, **136**, B864.; b) W. Kohn and L. J. Sham, *Phys. Rev.*, 1965, **140**, A1133.

38 M. C. Payne, M. P. Teter, D. C. Allan, T. A. Arias and J. D. Joannopoulos, *Rev. Mod. Phys.*, 1992, **64**(4), 1045.

39 S. Baroni, S. de Gironcoli, A. Dal Corso and P. Giannozzi, *Rev. Mod. Phys.*, 2001, **73**(2), 515.

40 X. Gonze and C. Lee, *Phys. Rev. B*, 1997, **55**(16), 10355.

41 a) J. P. Crocombette, F. Jollet, L. T. Nga and T. Petit, *Phys. Rev. B*, 2001, **64**(2), 104107; b) M. Freyss, T. Petit and J.-P. Crocombette, *J. Nucl. Mater.*, 2005, **347**(1-2), 44.

42 G. Beridze and P. M. Kowalski, *J. Phys. Chem. A*, 2014, **118**(50), 11797.

43 Y. Yun, D. Legut and P. M. Oppeneer, *J. Nucl. Mater.*, 2012, **426**(1-3), 109.

44 Q. Yin and S. Y. Savrasov, *Phys. Rev. Lett.*, 2008, **100**(22), 225504.

45 B.T. Wang, P. Zhang, R. Lizárraga, I. Di Marco and O. Eriksson, *Phys. Rev. B*, 2013, **88**(10), 104107.

46 a) Z.-G. Mei, M. Stan and J. Yang, *J. Alloys Compd.*, 2014, **603**, 282.; b) Z.-G. Mei, M. Stan and B. Pichler, *J. Nucl. Mater.*, 2013, **440**(1-3), 63.

47 S. L. Dudarev, D. N. Manh and A. P. Sutton, *Philos. Mag. B*, 1997, **75**(5), 613.

48 D. A. Andersson, G. Baldinozzi, L. Desgranges, D. R. Conradson and S. D. Conradson, *Inorg. Chem.*, 2013, **52**(5), 2769.

49 P. Nerikar, T. Watanabe, J. S. Tulenko, S. R. Phillpot and S. B. Sinnott, *J. Nucl. Mater.*, 2009, **384**(1), 61.

50 a) X.-D. Wen, R. L. Martin, L. E. Roy, G. E. Scuseria, S. P. Rudin, E. R. Batista, T. M. McCleskey, B. L. Scott, E. Bauer, J. J. Joyce and T. Durakiewicz, *J. Chem. Phys.*, 2012, **137**, 154707; b) X.-D. Wen, R. L. Martin, G.E. Scuseria, S. P. Rudin, E. R. Batista and A. K. Burrell, *J. Phys.: Condens. Matter*, 2013, **25**(2), 025501.

51 a) P. F. Weck, E. Kim, N. Balakrishnan, F. Poineau, C. B. Yeamans and K. R. Czerwinski, *Chem. Phys. Lett.*, 2007, 443(1-3), 82.; b) P. F. Weck, E. Kim, C. F. Jove-Colon and D. C. Sassani, *Dalton Trans.*, 2012, **41**, 9748.; c) P. F. Weck and E. Kim, *Dalton Trans.*, 2014, **43**, 17191.

52 a) S. Ostanin and P. Zeller, *J. Phys.: Condens. Matter*, 2007, **19**(24), 246108; b) S. Ostanin and P. Zeller, *Phys. Rev. B,* 2007, **75**(7), 073101.

53 a) L. C. Shuller, R. C. Ewing and U. Becker, *J. Nucl. Mater.*, 2013, **434**(1-3), 440.; b) L. C. Shuller, M. W. Bender, M. S. Walker and U. Becker, *Minerals*, 2014, **4,** 690.; c) L. C. Shuller, R. C. Ewing and U. Becker, *Am. Mineral.*, 2010, **95**, 1151.

54 a) P. J. Hay and R. L. Martin, *J. Chem. Phys.*, 1998, **109**, 3875.; b) P. J. Hay, R. L. Martin and G. Schreckenbach, *J. Phys. Chem. A*, 2000, **104**(26), 6259.

55 L. Castro, A. Yahia and L. Maron, *Chem. Phys. Chem.*, 2010, **11**(5), 990.

56 a) G. Schreckenbach and G. A. Shamov, *Acc. Chem. Res.*, 2010, **43**(1), 19.; b) G. A. Shamov, G. Schreckenbach and T.

N. Vo, *Chem. - Eur. J.*, 2007, **13**(17), 4932.; c) S. O. Odoh and G. Schreckenbach, *Inorg. Chem.*, 2013, **52**(9), 5590.
57 N. Iché-Tarrat and C. J. Marsden, *J. Phys. Chem. A*, 2008, **112**(33), 7632.
58 a) D. Majumdar, K. Balasubramanian and H. Nitsche, *Chem. Phys. Lett.*, 2002, **361**(1-2), 143.; b) D. Majumdar, S. Roszak, K. Balasubramanian and H. Nitsche, *Chem. Phys. Lett.*, 2003, **372**(1-2), 232.; c) D. Chaudhuri and K. Balasubramanian, *Chem. Phys. Lett.*, 2004, **399**(1-3), 67.
59 R. Vochten and M. Deliens, *Can. Mineral.*, 1998, **36**, 1077.
60 K. Walenta, *Mineral. Petrogr. Mitt.* , 1998, **56**, 167.
61 D. L. Clark, D. E. Hobart and M. P. Neu, *Chem. Rev.*, 1995, **95**(1), 25.
62 R. J. Finch and R. C. Ewing, *J. Nucl. Mater.*, 1992, **190**, 133.
63 I. Grenthe, J. Drożdżyński, T. Fujino, E. C. Buck, T. E. Albrecht-Schmitt and S. F. Wolf, in *The chemistry of the actinide and transactinide elements*, Springer Netherlands, 2008, pp. 253-698.
64 W. Marckwald, *Centralblatt Mineralogy*, 1906, **763**.
65 C. Frondel and R. Meyrowicz, *Am. Mineral.*, 1956, **41**, 127.
66 C. L. Christ, J. R. Clark and H. T. Evans, *Science*, 1955, **121**, 472.
67 C. L. Christ and J. R. Clark, *Am. Mineral.*, 1956, **41**, 844.
68 R. J. Finch, M. A. Cooper, F. C. Hawthorne and R. C. Ewing, *Can. Mineral.*, 1999, **37**(4), 929.
69 L. J. Bonales, C. Menor-Salván and J. Cobos, *J. Nucl. Mater.*, 2015, **462**, 296.
70 MaterialsStudio,*http://accelrys.com/products/ materials-studio*, 2014.
71 J. P. Perdew, K. Burke and M. Ernzerhof, *Phys. Rev. Lett.*, 1996, **77**, 3865.
72 J. P. Perdew, A. Ruzsinszky, G. I. Csonka, O. A. Vydrov, G. E. Scuseria, L. A. Constantin, X. Zhou and K. Burke, *Phys. Rev. Lett.*, 2008, **100**, 136406.
73 S. Grimme, *J. Comput. Chem.*, 2006, **27**(15), 1787.
74 B. G. Pfrommer, M. Côté, S. G. Louie and M. L. Cohen, *J. Comput. Phys.*, 1997, **131**(1), 233.
75 H. J. Monkhorst and J. D. Pack, *Phys. Rev. B*, 1976, **13**(12), 5188.
76 N. Troullier and J. L. Martins, *Phys. Rev. B,* 1991, **43**(3), 1993.
77 M. Fuchs and M. Scheffler, *Comput. Phys. Commun.*, 1999, **119**(1), 67.
78 L. Kleinman and D. M. Bylander, *Phys. Rev. Lett.*, 1982, **48**(20), 1425.
79 P. Haynes and K. Refson, *cpi2recpot: Converts from .cpi format generated by fhi98PP to the recpot format used by CASTEP and ONETEP*, 2007.
80 R. T. Downs, K. L. Bartelmehs, G. V. Gibbs and M. B. Boisen, *Am. Mineral.*, 1993, **78**, 1104.
81 J. D. Martin, *XPowder12, Ver. 04.13*, 2012.
82 ICDD, *The international center for diffraction data. PDF-2 database*, 2003.
83 E. del Corro Garcia, PhD. Thesis, Universidad Complutense de Madrid. CC. Químicas Departamento de Química Física I, 2011.
84 J. Cejka and Z. Urbanec, *Casopis Narodniho Muzeo*, 1988, **157**, 1-10.
85 J. Cejka, *Rev. Mineral. Geochem.*, 1999, **38**, 521.
86 H. R. Hoekstra and S. Siegel, *J. Inorg. Nucl. Chem.*, 1973, **35**(3), 761.
87 J. G. Catalano and G. E. Brown, *Am. Mineral.*, 2004, **89**, 1004.